Biochemistry and Biophysics Reports 7 (2016) 386–393

Contents lists available at ScienceDirect

Biochemistry and Biophysics Reports

journal homepage: www.elsevier.com/locate/bbrep

Sulfmyoglobin conformational change: A role in the decrease of oxy-myoglobin functionality

Elddie Román-Morales, Erika López-Alfonzo, Ruth Pietri, Juan López-Garriga *

Department of Chemistry, University of Puerto Rico, Mayagüez Campus, PO BOX 9019, Mayagüez, Puerto Rico 00681-9019

ARTICLE INFO

Article history:
Received 25 January 2016
Received in revised form
28 June 2016
Accepted 1 July 2016
Available online 7 July 2016

Keywords:
Sulfmyoglobin (SMb)
Myoglobin (Mb)
Hemoglobin I (HbI)
Hydrogen sulfide (H_2S)
SAXS
WAXS

ABSTRACT

This work is focused at understanding the interaction of H_2S with Myoglobin (Mb), in particular the Sulfmyoglobin (SMb) product, whose physiological role is controversial and not well understood. The scattering curves, Guinier, Kratky, Porod and *P(r)* plots were analyzed for oxy-Mb and oxy-Hemoglobin I (oxyHbI) in the absence and presence of H_2S, using Small and Wide Angle X-ray Scattering (SAXS/WAXS) technique. Three dimensional models were also generated from the SAXS/WAXS data. The results show that SMb formation, produced by oxyMb and H_2S interaction, induces a change in the protein conformation where its envelope has a very small cleft and the protein is more flexible, less rigid and compact. Based on the direct relationship between Mb's structural conformation and its functionality, we suggest that the conformational change observed upon SMb formation plays a contribution to the protein decrease in O_2 affinity and, therefore, on its functionality.

1. Introduction

Hydrogen Sulfide (H_2S) is a gas with a "rotten egg" like smell produced in different systems in nature and industrial processes [1,2]. Through the years, H_2S was known as a toxic gas that disrupts the respiratory process by inhibition of the cytochrome c oxidase (CcO) [1–5]. It also forms sulfhemoglobinemia, a rare blood condition with anemic/cyanotic symptoms, induced by the increase concentration of Sulfmyoglobin (SMb) and Sulfhemoglobin (SHb) complexes [5–9]. However, another side of the H_2S molecule arose when it was discovered that there were three proteins [cysthathionine β-synthase (CBS), cysthathionine γ-lyase (CSE), and 3-mercaptopyruvate sulfur transferase (MST)] that produced H_2S physiologically and were present in different parts of the human body [1–5]. Different cytoprotective roles have been associated to H_2S in the respiratory, vascular, nervous, endocrine and gastrointestinal systems [1–5]. For this reason, H_2S has been evaluated as a potential therapeutic tool for the treatment of multiple diseases [10,11]. Nevertheless, the concept of H_2S therapy should be treated with caution since there is a thin line between its cytoprotective and cytotoxic aspects defined by concentration. The H_2S physiological concentration has been suggested to be low, ranging from nM to μM [1–3]. When a person is exposed to high H_2S concentration, there is an increase in physiological H_2S concentration that leads to the cytotoxic effects dominating over cytoprotective [2]. This is important when developing an efficient therapeutic tool, where the beneficial effects are maximized and the harmful effects minimized. The process for developing a resourceful H_2S therapy requires a better understanding of the chemistry of H_2S with different systems, in particular, protein interaction with this molecule.

Our research is focused at understanding one of the products of the interaction of H_2S with hemeproteins, in particular the sulfheme proteins (SMb and SHb), whose physiological role is controversial and not well understood. When myoglobin (Mb) and hemoglobin (Hb) are exposed to H_2S in the presence of oxygen (O_2) or hydrogen peroxide (H_2O_2), a sulfur atom incorporates across the β-β double bond of the pyrrole B, as shown in Fig. 1 [7,8]. This sulfur ring formation can be identified by its characteristic absorption bands around 620 or 715 nm, depending on the bound-ligand and oxidation state of the heme-iron [7]. Resonance Raman is another tool for the recognition of the sulfheme complex formation by evaluation of the vinyl modes bands (1620 and 1026 cm^{-1}) and the satellites bands around υ_4 [7,8]. Moreover, the presence of a properly oriented distal His residue is crucial for the sulfheme complex formation. This was determined by analyzing the H_2S reactive Hemoglobin I (HbI) from the clam *Lucina pectinata* that interestingly does not form the sulfheme complex, given that it lacks of a distal His residue [7,8]. When the sulfheme complex forms, Mb decreases its O_2 affinity by approximately 2500 folds. This significant decrease in O_2 affinity was

* Corresponding author.
E-mail address: juan.lopez16@upr.edu (J. López-Garriga).

http://dx.doi.org/10.1016/j.bbrep.2016.07.002

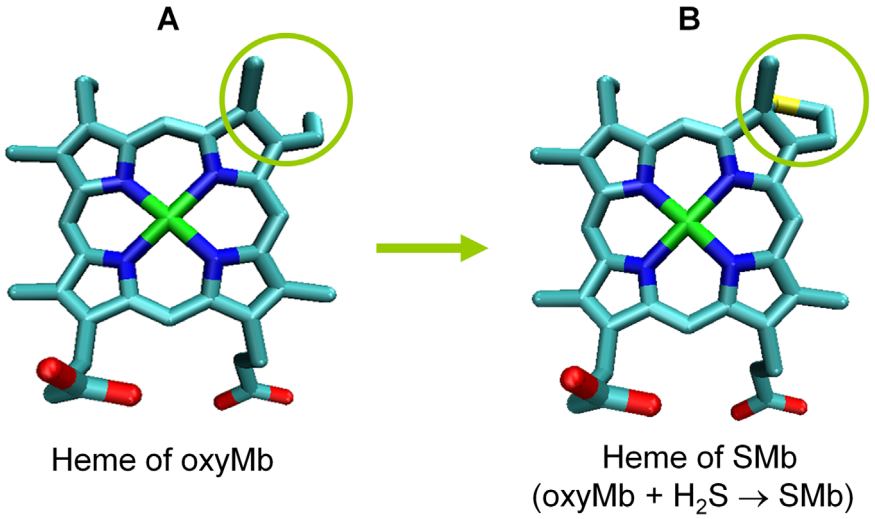

Fig. 1. Sulfmyoglobin (SMb) Structure. Myoglobin (A, left) and SMb isomer C (B, right); PDB files 1MBO (Mb) and 1YMC (SMb).

determined by comparing the 50% oxygenation values in the oxygen binding curve of Mb and SMb (0.79 and 0.00028 atm, respectively) [12]. Berzofsky et al. determined the local chemical change that plays a part in the decrease of the protein functionality. They evaluated the bond strength of the heme Fe-ligand of Mb and SMb by IR studies. A 10 cm^{-1} red-shift was observed in the IR spectra of the SMb complex, representative of a decrease in electron density, bond order and strength of the heme-ligand interaction. They attributed this to the electron withdrawing effect of the sulfur atom in the heme macrocycle, resulting in a decrease in electron density of the Fe. As a consequence, the heme-Fe^{II} acquired a character of heme-Fe^{III}; thus, weakening the Fe-ligand bond since the metal-ligand π contribution is compromised. This is also favored by the rupture of the heme group conjugation produced by the heme distortion, as result of the sulfur ring incorporation [12,13]. Moreover, Berzofsky et al. suggested that a 0.5 cm^{-1} shift corresponds to a decrease in O_2 affinity by a factor of 10, which indicates that this local chemical structural change contributes to only a 200 fold decrease in O_2 affinity [12], representing only 8% of the total decrease in affinity (2500 folds) determined by the oxygen binding curve. Therefore, there are other significant changes occurring in the protein as a consequence of the sulfheme complex formation that also contribute to the decrease in protein functionality.

2. Material and methods

2.1. Sample preparation

Myoglobin (Mb) from equine heart was purchased from Sigma-Aldrich. Recombinant HbI (rHbI) was prepared and purified as previously reported [23] and used as control. Both proteins were dissolved in a 100 mM Succinic Acid, 100 mM Potassium dihydrogen phosphate, and 1 mM EDTA buffer, 6.5 pH (all purchased in Sigma-Aldrich). The oxy-derivatives were prepared by adding [1:15] concentration ratio of [protein: sodium dithionite] under anaerobic conditions followed by O_2 purging [4]. The H_2S solution was prepared by dissolving sodium sulfide (purchased in Alfa-Aesar) in the previously mention anaerobic buffer. The sulfheme complex formation was monitored through its characteristic 620 nm band by UV–vis spectroscopy using an Agilent 8453 spectrophotometer [8]. The sulfheme complex was acquired by adding H_2S to the oxyMb complex in a [1:70] concentration ratio of [oxyMb: H_2S] that provides the highest intensity and stability of the 620 nm characteristic band.

2.2. SAXS/WAXS data acquisition and processing

SAXS/WAXS data were recorded on oxyMb and oxyHbI in the absence and presence of H_2S. The 620 nm band was monitored before and after data acquisition for both proteins. The band was only detected in oxyMb after addition of H_2S since oxyHbI does not form the sulfheme derivative. The 100 mM succinic acid, 100 mM potassium dihydrogen phosphate, and 1 mM EDTA buffer was used as a background. In the absence of H_2S, the scattering data of oxyMb were first collected at 5, 6, 10, and 11 mg/mL. The optimal protein concentration was found to be 11 mg/mL and the scattering data in the presence of H_2S were therefore collected at this concentration. For HbI the final protein concentration was 6.7 mg/mL. The SAXS/WAXS data was collected simultaneously at the X-9 Beamline of the National Synchrotron Light Source at Brookhaven National Laboratory using a PILATUS 300k SAXS detector and a Photonic Science CCD WAXS detector [24]. For triplicated data acquisition, 20 μL of sample was continuously flowed through a 1-mm diameter capillary where it was exposed to the x-ray beam for 30 s. Initial data processing was performed using the pyXS-v2 software package developed at X9. The program converted the two-dimensional scattering patterns recorded on the SAXS/WAXS detectors into one-dimensional scattering profiles. Three scattering patterns of each sample were obtained, averaged, and buffer (background) subtracted. Further SAXS/WAXS data processing and analysis were performed using 2.5.2 ATSAS Package [25,26]. Guinier, Kratky and Porod [20] analyses were conducted using Primus [27] The pair distribution functions were evaluated using GNOM [28]. 3-D surfaces were generated using DAMMIN [29], averaged using DAMAVER [30], and superimposed using SUPCOMB [31]. The theoretical scattering profiles of oxyMb and SMb atomic models were evaluated using CRYSOL [32]. Pymol was used for graphical visualization and figure generation.

3. Results and discussion

Characterization of oxyMb and oxyHbI with and without H_2S was conducted using their overall dimensions and shapes, as well as their internal structural features derived from SAXS and WAXS scattering data, respectively.

3.1. Scattering curve and Guinier plot

In SAXS/WAXS, the intensity of the scattered X-ray beam is

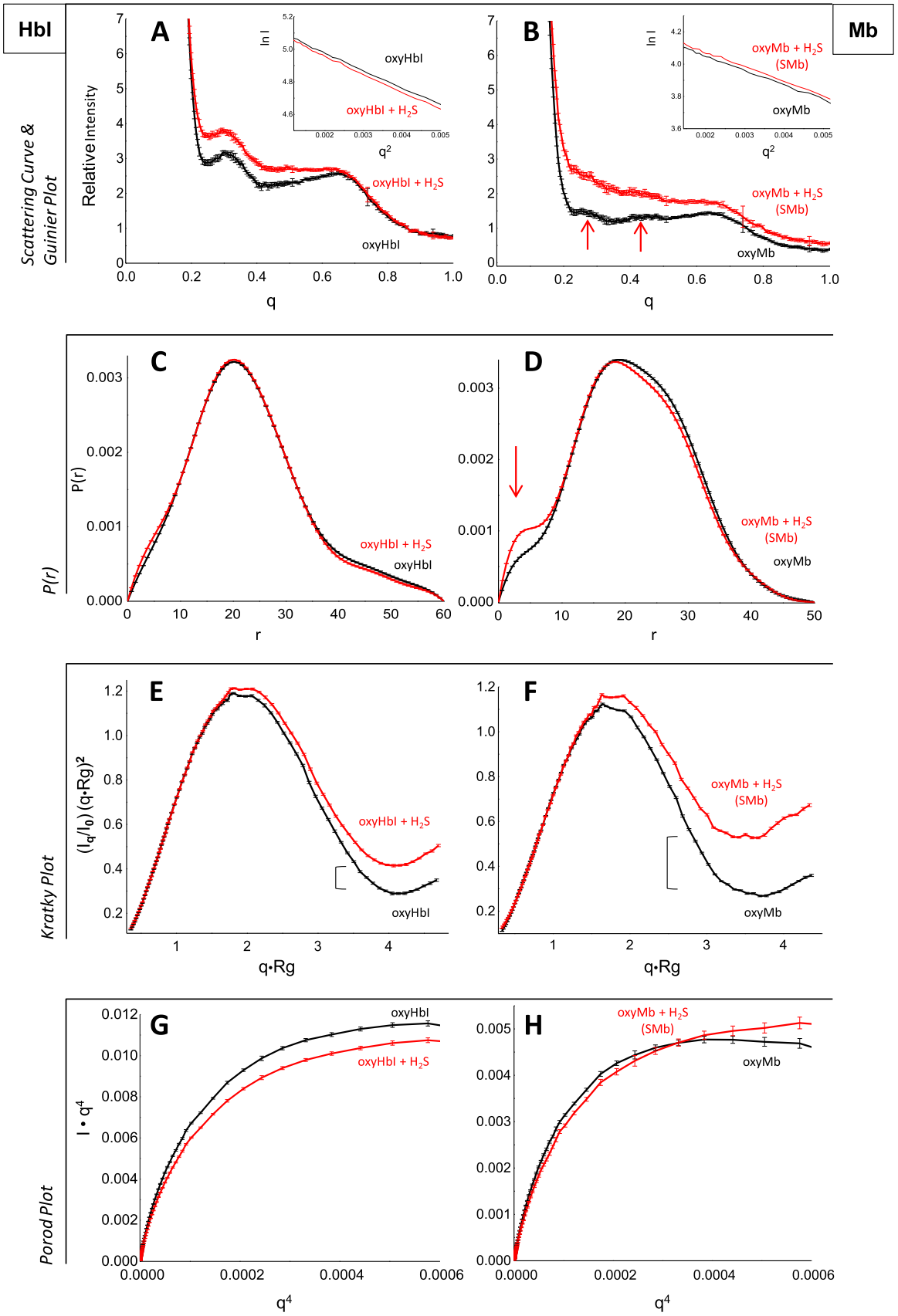

Fig. 2. SAXS and WAXS analysis. Left panel is oxyHbI in the absence (black line) and presence of H_2S (red line). Right panel is oxyMb (black line) and SMb (red line, product of oxyMb and H_2S interaction). A and B; SAXS/WAXS scattering curves (showing q range of 0.19–1.0 $Å^{-1}$), with their corresponding Guinier Plot (inset; q range =0.030–0.072 $Å^{-1}$ for HbI and 0.038–0.072 $Å^{-1}$ for Mb). C and D; *P(r)* plots normalized to *I(0)* (q range =0.024–0.442 $Å^{-1}$ for oxyHbI, 0.039–0.44 $Å^{-1}$ for oxyHbI in the presence of H_2S, 0.025–0.5 $Å^{-1}$ for oxyMb and 0.036–0.05 $Å^{-1}$ for SMb). E and F; Dimensionless *Kratky* plots (q range =0.02–0.26 $Å^{-1}$). G and H; *Porod* plots (q range =0.02–0.16 $Å^{-1}$). (For interpretation of the references to color in this figure legend, the reader is referred to the web version of this article.)

measured as a function of the momentum transfer vector q, ($q=4\pi sin\theta)/\lambda$), where θ is the scattering angle and λ is the beam wavelength [19,26]. The transfer vector q is inversely related to the real space distance between scattering centers d within the particle ($q = 2\pi/d$) [19,26]. Thus, the low q region in the scattering pattern ($\sim$0.01–0.05 Å^{-1}) represents vectors of length $\sim$600–100 Å and differences in the intensity within this region would reflect changes in the overall shape of the molecule. Conversely, at higher q, the length space distance d between centers become smaller and changes in this region suggest fluctuations in internal structural features [18,22]. Overall, it can be generalized that an increase in protein fluctuations or mobility is illustrated by a decrease in the definition or sharpness of peaks, in the high q region of the scattering curve of the protein [18,22,33,34].

Fig. 2A shows the scattering curves ($I(q)$ vs q) of the oxyHbI complex in the absence (black line) and presence of H_2S (red line). The HbI scattering curves maintain the same scattering central maxima in the presence or absence of H_2S. This indicates that the overall shape and internal structure of the protein remain unchanged in the presence of H_2S. Fig. 2B illustrates the scattering curves of oxyMb (black line) in the presence of H_2S, which leads to the formation of the SMb complex (red line). In addition to an evident increase in protein mobility and fluctuations characterized by a decrease in peak definition and sharpness, a noticeable fading of the scattering peaks at $\sim$0.27 and 0.43 Å^{-1} was observed upon SMb complex formation. When comparing the scattering curves of Mb and HbI after addition of H_2S, the scattering pattern with the greatest degree of change is that observed for Mb (e.g. q region at 0.27–0.43 Å^{-1}) as a result of SMb complex formation. It is important to mention that oxyHbI reacts with H_2S to form ferric hemoglobin sulfide in which H_2S coordinates to the ferric heme iron (Fe^{III}-H_2S) most probably by nucleophilic displacement of the bound superoxide [35]. In contrast, reaction of oxyMb with H_2S modifies the heme active center (Fig. 1) producing SMb [7,8]. Thus, the data indicate that H_2S binding to the ferric heme in oxyHbI does not induces significant global and internal structural changes, while modification of the heme macrocycle in oxyMb produces internal structural fluctuations. Overall, SMb shows greater variation of structural conformational changes upon interaction with H_2S, as evidence by the loss of scattering peaks. The structural distances that were present in oxyMb (represented by the scattering peaks at 0.27 and 0.43 Å^{-1}or d space of $\sim$23–15 Å) are no longer the most abundant as a consequence of the structural conformational change associated to the SMb complex. Interestingly, time resolved X-ray scattering data on MbCO showed that the disappearance of the peaks in these regions was due to tertiary structural relaxation, specifically to displacement of the E and F helices [36]. It is therefore plausible that SMb induce changes in these helices as well.

One parameter that can be determined directly from the SAXS data in the low q region ($\sim$0.01–0.05 Å^{-1}) is the radius of gyration or R_g, using the Guinier approximation [19,26]. The R_g is the root mean square distance of an object from its center of mass and provides a measure of the overall size of the protein. According to the Guinier approximation, at very small q ($q < 1.3/R_g$) a plot of ln $I(q)$ versus q^2 should be linear for a globular protein (Eq. (1)). From the slope of the linear fit one can determine the R_g and hence the overall size of the protein. In addition, deviations from linearity in the Guinier plots indicate aggregation [19,26]. The insets in Fig. 2A and B show the Guinier plots for oxyHbI and oxyMb in the absence and presence of H_2S. The linearity of the Guinier plots of both proteins with and without H_2S indicates no detectable aggregation. As shown in Table 1, the R_g of oxyHbI was determined to be $\sim$18.0 Å and no change in this value was detected after exposure of H_2S. Similarly, the R_g of oxyMb and SMb were determined to be 16.8 and 16.7 Å, respectively, indicating similar overall sizes [19].

Table 1
Structural parameters determined by Guinier approximation and indirect Fourier transformation of SAXS/WAXS data.

Protein	$R_{g\ (Guinier)}$ (Å)	$R_{g\ (Gnom)}$ (Å)	D_{max} (Å)
oxyHbI	17.90 ($\pm$0.06)	18.16 ($\pm$0.04)	60
oxyHbI + H_2S	18.10 ($\pm$0.66)	17.81 ($\pm$0.05)	60
oxyMb	16.80 ($\pm$0.13)	16.32 ($\pm$0.04)	50
SMb (oxyMb + H_2S)	16.70 ($\pm$0.38)	15.98 ($\pm$0.02)	50

$$I(q) = I(0)exp(-1/3R_g^2q^2) \quad (1)$$

3.2. Pair distribution function, P(r)

The shapes and maximum dimensions (D_{max}) of proteins can also be determined directly from their SAXS/WAXS scattering data. Indirect Fourier transformation of the scattering data $I(q)$ yields a pair distribution function $P(r)$, which is a histogram of distances between pairs of elements within the entire volume of the scattering protein (Eq. (2)) [19,26]. In general, the $P(r)$ function is a real space representation of the scattering data and provides an approximation of the shape and dimension of a protein in solution. For example, globular proteins have a symmetric bell-shaped $P(r)$, whereas unfolded particles have an extended tail. In addition, multi-domain proteins often yield $P(r)$ with multiple shoulders and oscillations corresponding to intra an inter-subunit distances [19,26].

$$P(r) = \frac{r^2}{2\pi^2}\int_0^\infty q^2 I(q)\frac{sinqr}{qr}dq \quad (2)$$

Fig. 2C shows the $P(r)$ plots of oxyHbI in the absence (black line) and presence of H_2S (red line). The contours of the $P(r)$ plots are characteristic of a globular protein with somewhat elongated sphere envelope [19]. There is no significant change in the $P(r)$ plot of oxyHbI after the protein has interacted with H_2S, indicating that the presence of H_2S does not alter significantly the envelope or structural conformation of HbI. Fig. 2D shows the $P(r)$ plots of oxyMb (black line) and SMb, formed after interaction of oxyMb with H_2S (red line). Interestingly, the Mb conformation upon SMb complex formation shows a new $P(r)$ contour with two distinct peaks. This is characteristic of two predominant regions within the overall globular conformation, as observed for calmodulin and thrombin-like enzymes [21,37]. Thus, the data suggest that SMb induces internal structural fluctuations, generating two distinctive regions within the overall dimension of the protein [21,37–39] without inducing a significant change in the overall protein dimension (D_{max}) [38,40]. Similar $P(r)$ profiles have been reported for *Rhinodrilus alatus* and *Glossoscolex paulistus* hemoglobins at basic pH and in the presences of urea respectively. The authors associated the two peaks to unfold and flexible forms of the proteins [41,42]. In addition, $P(r)$ plots displaying two peaks in their contours have been suggested for proteins with U-shape or two-domain envelopes [19,21,37]. In this case, it is more likely that the Mb envelope acquires a very small degree of a U-shape or cleft in its global shape upon SMb complex formation. The suggested increase in fluctuation or flexibility observed in the $P(r)$ plot can be profoundly evaluated using Kratky and Porod plots.

3.3. Kratky and Porod plots

SAXS/WAXS data is also commonly used to identify protein flexibility. Proteins that vary in flexibility and conformation can be recognized from the scattering data using the Kratky and Porod plots defined by the following equation [20]:

$$V_p = 2\pi^2 I(0)/Q \quad Q = \int_0^\infty q^2 I(q)dq \tag{3}$$

V_p is the hydrated particle volume (e.g. protein) and Q is the Porod invariant, a direct measurement of the density contrast [20]. According to the Kratky analysis, a plot of $q^2I(q)$ vs q should display a bell-shape with a clear maximum for compact globular proteins. Proteins with dual structure (compact and flexible regions) will show at low q a maximum that resembles the order region within the ensemble and at higher q a "tail" that represents the disordered or flexible region [19,20,40,43,44]. With increasing protein flexibility, the "tail" segment of the Kratky plot will raise, indicating an increase in disordered/flexible structure within the protein conformation. For example, a completely unfolded protein will exhibit a plateau "tail" [40,43,45]. On the other hand, the Porod approximation states that a plot of $q^4I(q)$ vs q^4 should display crescent-hyperbolic tendency arriving to a plateau as q increases for compact globular proteins. The loss of plateau suggests an increase in protein flexibility [20,40]. Overall, Kratky and Porod plots are employed to qualitatively assess the relationship between flexibility and protein volume. Proteins that posses a dual structure with compact and flexible regions within their structural domain can be identified using both approximations [20,40].

Fig. 2E shows the Kratky plots of oxyHbI in the absence (black line) and presence of H_2S (red line). A bell-like shape was observed, demonstrating a compact globular protein with some flexibility represented by a "tail" at higher q. The tail rises a little when HbI is in the presence of H_2S, implying an increase in protein flexibility produced by H_2S. Fig. 2F shows the Kratky plots of oxyMb (black line) and SMb formed by the interaction of oxyMb with H_2S (red line). It also shows a bell-shape with a "tail", indicating a compact globular protein with some flexibility. However, SMb formation clearly produces a "tail" that rises even more. This suggests that the SMb complex induces a greater change in the protein structural conformation where a significant increase in packing flexibility in acquired.

Fig. 2G shows the Porod plots of oxyHbI in the absence (black line) and presence of H_2S (red line). The plots demonstrate the classical hyperbolic shape curve arriving to a plateau as q increases, before and after H_2S exposure, indicating no significant change in protein flexibility. Fig. 2H shows the Porod plots of oxyMb (black line) and SMb formed by the interaction of oxyMb with H_2S (red line). OxyMb demonstrates a classical hyperbolic shape curve arriving to a plateau as q increases, characteristic of a globular, compact, and rigid conformation. Interestingly, once the SMb complex is formed, a loss in the plateau is observed representative of a gain in conformational flexibility that is not observed in HbI upon H_2S exposure. This change in protein structural conformation, specifically induced by the SMb formation, is different from the structural change induced by ligand migration towards the protein active site, given that: (1) before H_2S exposure, the protein was in a O_2 saturated environment where structural changes associated to ligand migration through the protein had already occurred and (2) both proteins had the same H_2S exposure. Regarding this, the distinction in the Kratky and Porod plot's of both proteins, when expose to H_2S, is due to the SMb formation since HbI does not form the sulfheme complex [7,8].

Overall, the scattering curves of SMb showed that the peaks at $q > 0.2$ are practically unresolved, indicating an increase in protein fluctuations and mobility as a consequence of SMb complex formation. The two peaks in the SMb $P(r)$ plot demonstrated changes in internal structural conformation, suggesting formation of a small cleft on the protein envelope with a two distinctive flexible

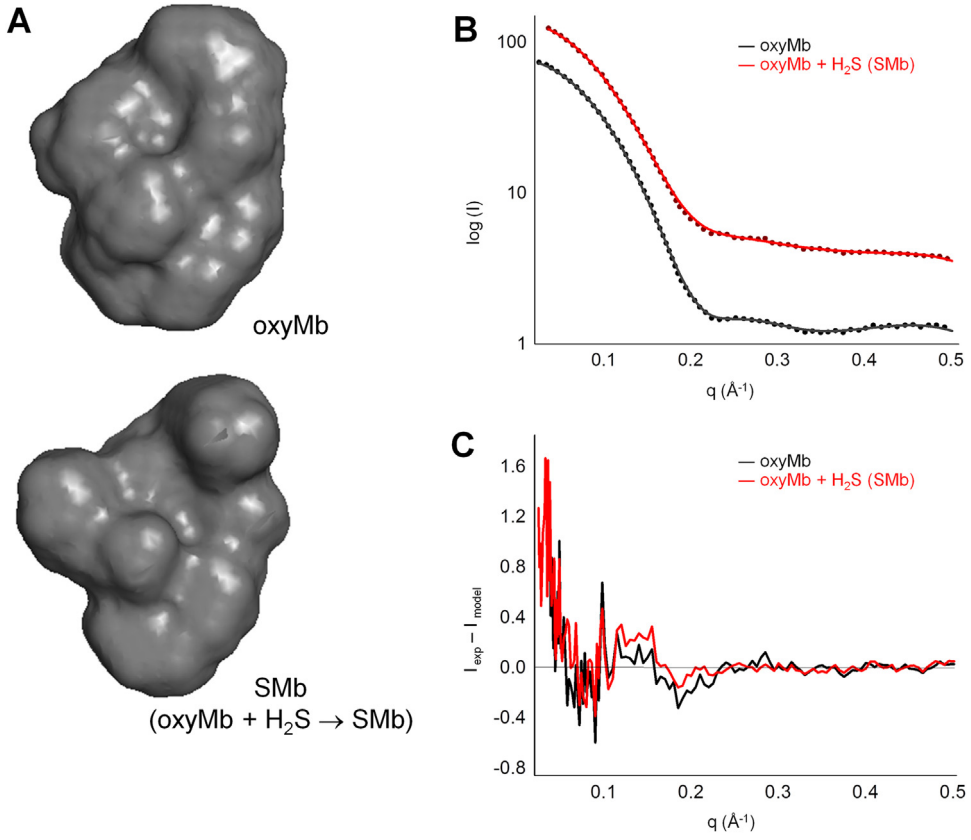

Fig. 3. SAXS/WAXS three dimensional models. A; SAXS/WAXS three-dimensional surfaces of oxyMb (top-left) and SMb (bottom-left). B; Comparison of the experimental SAXS/WAXS data of oxyMb (black-dotted lines) and SMb (red-dotted lines) with the corresponding calculated scattering curves of their theoretical models (solid lines). The q range used for the theoretical models was the same as those used in the $P(r)$ function. The curves were offset for better appraisal (oxyMb has $x^2=0.8$ and $R^2=0.99984$; SMb has $x^2=2.2$ and $R^2=0.99975$). C; Residual plots of the experimental minus the calculated scattering curves of oxyMb (black line) and SMb (red line) theoretical models.

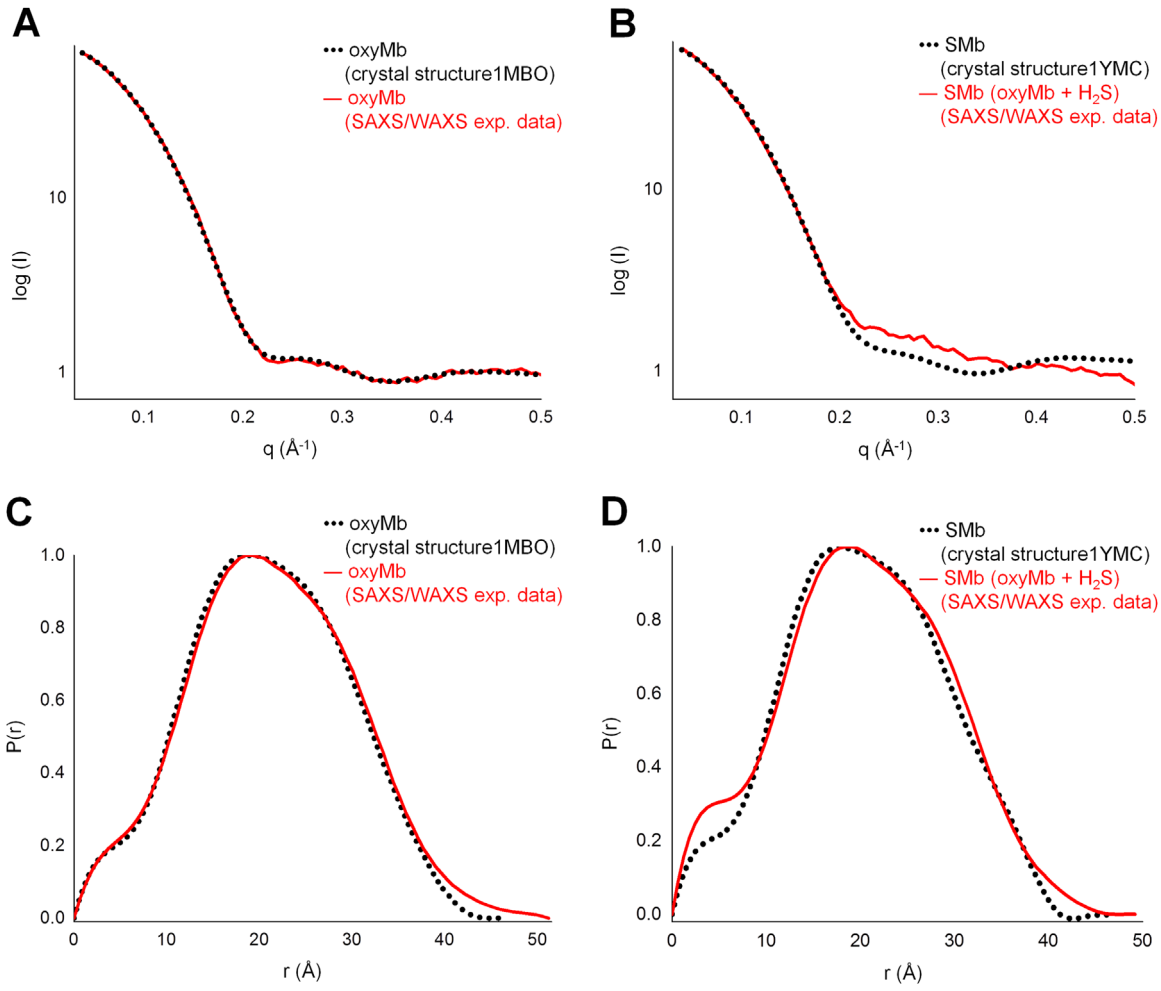

Fig. 4. Comparison of the SAXS/WAXS and crystallographic data. Left panel is oxyMb from the SAXS/WAXS experimental data (red-line) and crystal structure (black-dotted line), PDB file 1MBO. Right panel is SMb from the SAXS/WAXS experimental data (red-line) and crystal structure (black-dotted line), PDB file 1 YMC. A and B; Scattering curves. C and D; The corresponding P(r) plots.

regions. The Kratky and Porod plots supports increase in flexibility, decrease in rigidity and compactness.

3.4. Three dimensional models and scattering from high resolution models

To acquire a visual perspective of the global surface features of SMb conformational effect, three-dimensional surfaces from SAXS/WAXS scattering data were produced for oxyMb and SMb. The three-dimensional scattering surfaces of the proteins were generated using the Dummy Atom Model Minimization method [29]. The algorithm represents a protein as a collection of dummy atoms in a constrained volume with a maximum diameter defined experimentally by D_{max}. It employs simulated annealing to generate the three-dimensional surface, and it calculates the scattering curve of the surface to evaluate its discrepancy (χ^2) with the experimental data (Eq. (4)) [19].

$$\chi^2 = \frac{1}{N-1}\sum_{i=1}^{N}\left(\frac{I_{exp}(q_i) - cI_{calc}(q_i)}{\sigma(q_i)}\right)^2 \quad (4)$$

Here $I_{exp}(q)$ and $I_{calc}(q)$ are the experimental and computed profiles, respectively, $\sigma(q)$ is the experimental error of the measured profile, N is the number of points in the profile, and c is the scaling factor.

Fig. 3A shows the surfaces of oxyMb and SMb, formed by the interaction of oxyMb with H_2S. The surfaces demonstrated general globular structures and reveal differences in their shapes, where the SMb envelope has a small cleft with two distinct regions. As shown in Fig. 3B, the scattering curves of the three-dimensional surfaces fit the experimental data well, yielding χ^2 values of 0.8 and 2.1 for oxyMb and SMb, respectively. This was also confirmed by the residual analysis of the experimental and calculated scattering curves (Fig. 3C), yielding R^2 values of 0.9998 and 0.9997 for oxyMb and SMb, respectively.

This local change was not observed in the SMb crystallographic structure probably due to the protein constriction that can occur during the process of crystal formation, which does not take place in SAX/WAXS since it is in solution. To corroborate this interpretation, the theoretical scattering curves of oxyMb and SMb atomic models (PDB ID:1MBO and 1YMC, respectively) were obtained using CRYSOL software [32]. The program uses multipole expansion for fast calculation of spherically averaged scattering profile and takes into account the hydration shell. It also compares the theoretical scattering curve with the SAXS/WAXS experimental data by fitting the curves and minimizing the discrepancy. The theoretical scattering curves obtained from the PDB structures were further analyzed to calculate the corresponding theoretical *P (r)* functions. In general, an atomic model that provides a good fit to the data is considered a valid description of the structure in solution.

As Fig. 4A shows, the theoretical scattering curve of oxyMb

atomic model fits the SAXS/WAXS experimental data well, implying similarities of both crystal and solution structures. The corresponding *P(r)* functions support the above suggestion (Fig. 4C). However Fig. 4B demonstrates that the theoretical scattering curve of SMb crystal structure poorly correlates with the scattering data of SMb in solution, indicating that the atomic model does not describe well the protein in solution. In fact, the peak at ~4 Å is not so well defined in the theoretical *P(r)* function of SMb atomic model, as shown in Fig. 4D, suggesting that the internal structural fluctuations are hampered by crystal packing forces, which limit the range of conformational motion accessible to the protein.

3.5. Conclusion and further outlooks

Taken together, the data suggest that SMb complex induces a conformational change increasing protein flexibility and fluctuations with decreasing rigidity. This change is specific of SMb and different from conformational change produce by ligand migration or heme Fe-ligand binding. Regarding this, the Mb's Xe cavities have been demonstrated to play a crucial role in the protein functionality by regulating ligand entry and release from the active site [14–16]. The ligand migration in the cavity produces a structural expansion of the cavity itself follow-on by gating motions of the surrounding residues that leads to a self opening of the migrating channel [16]. The cavity comes back to its original volume once the ligand has left the cavity, mimicking a breathing motion [16,17]. The final channel is created by the rotating motion of the distal His opening the gate toward the active heme site [16]. Any change in the size and shape of these pockets directly affects the Mb function, which results in significant physiological effects [14–16]. Olson et al. [15] demonstrated that a decrease in the size of the cavity produced a more rigid and compact packing. As a result, it lowers the rate of ligand capture by making it difficult for the ligand to arrive to the active site. However, if the ligand is able to arrive to the active site, dissociation is even more difficult since the ligand is "trapped" in the active site, leading to an overall increase in O_2 affinity [15]. Upon SMb formation, the opposite is observed, a decrease in O_2 affinity. On this basis, we propose that the observed changes in conformation and increase in protein flexibility play a role in the decrease in O_2 affinity by SMb, in addition to the reported local structural change on the heme. These structural changes would facilitate ligand entry but destabilize even more ligand bonding, leading to an overall decrease in O_2 affinity.

Furthermore, in addition to the heme-Fe ligand transport, it has been suggested that the conformational cavities are capable of carrying additional ligands, such as NO, giving Mb higher carrying capacity than (1:1) stoichiometry and further physiological roles (e.g. scavenger) [14–17,46]. In this study we demonstrated that the inner structure of Mb is altered by the formation of SMb by increasing protein flexibility, movement, and fluctuation. On this basis, considering the constant ligand competition and the increase in protein flexibility of SMb, enhancement of H_2S entry and O_2 displacement may be possible. This could lead to a plausible H_2S transports flux, in addition to the known rapid diffusive flux of free H_2S.

The nature of the proteins should be further studied, given that, it is intriguing that a protein whose functionality is H_2S transport does not suffer a significant conformational change while a protein whose "main functionality" is O_2 storage and transport suffers significant conformational change, when exposed to H_2S. Furthermore, it opens the door to explore the conformation change associated with the reaction of oxy-Hemoglobin with H_2S, which only shows a decrease in O_2 affinity of 135 folds [47], suggesting that cooperativity may play an important role in protecting oxy-Hemoglobin functionality.

Acknowledgment

This work was supported in part by funds from the NSF (Grant 0843608), and fellowships from NIH-RISE2Best (Grant R25GM088023), and Alfred P. Sloan (NACME Grant 2010-3-02). We thank Dr. Lisa Miller, Mr. Vito Graziano, and Dr. Mark Allaire for the X9-SAXS/WAXS facilities at NSLS.

This research used resources of beamline X9 of the National Synchrotron Light Source, a U.S. Department of Energy (DOE) Office of Science User Facility operated for the DOE Office of Science by Brookhaven National Laboratory under Contract No. DE-AC02-98CH10886.

Appendix A. Transparency document

Supplementary data associated with this article can be found in the online version at http://dx.doi.org/10.1016/j.bbrep.2016.07.002.

References

[1] A. di Masi, P. Ascenzi, H2S: a "double face" molecule in health and disease, BioFactors 39 (2) (2013) 186–196.
[2] K.R. Olson, K.D. Straub, The role of hydrogen sulfide in evolution and the evolution of hydrogen sulfide in metabolism and signaling, Physiology 31 (1) (2016) 60–72.
[3] L. Li, P.K. Moore, Putative biological roles of hydrogen sulfide in health and disease: a breath of not so fresh air? Trends Pharmacol. Sci. 29 (2) (2008) 84–90.
[4] R. Pietri, A. Lewis, R.G. Leon, G. Casabona, L. Kiger, S.R. Yeh, S. Fernandez-Alberti, M.C. Marden, C.L. Cadilla, J. Lopez-Garriga, Factors controlling the reactivity of hydrogen sulfide with hemeproteins, Biochemistry 48 (22) (2009) 4881–4894.
[5] R. Pietri, E. Roman-Morales, J. Lopez-Garriga, Hydrogen sulfide and hemeproteins: knowledge and mysteries, Antioxid. Redox Signal. 15 (2) (2011) 393–404.
[6] K. Murphy, C. Ryan, E.M. Dempsey, P.W. O'Toole, R.P. Ross, C. Stanton, C. A. Ryan, Neonatal sulfhemoglobinemia and hemolytic anemia associated with intestinal *Morganella morganii*, Pediatrics 136 (6) (2015) e1641–e1645.
[7] B.B. Rios-Gonzalez, E.M. Roman-Morales, R. Pietri, J. Lopez-Garriga, Hydrogen sulfide activation in hemeproteins: the sulfheme scenario, J. Inorg. Biochem. 133 (2014) 78–86.
[8] E. Roman-Morales, R. Pietri, B. Ramos-Santana, S.N. Vinogradov, A. Lewis-Ballester, J. Lopez-Garriga, Structural determinants for the formation of sulfhemeprotein complexes, Biochem. Biophys. Res. Commun. 400 (4) (2010) 489–492.
[9] M. Noor, E. Beutler, Acquired sulfhemoglobinemia. An underreported diagnosis? West. J. Med. 169 (6) (1998) 386–389.
[10] D. Wu, Q. Hu, Y. Zhu, Therapeutic application of hydrogen sulfide donors: the potential and challenges, Frontiers of Medicine, 2015.
[11] Y. Zheng, X. Ji, K. Ji, B. Wang, Hydrogen sulfide prodrugs-a review, Acta Pharm. Sin. B 5 (5) (2015) 367–377.
[12] J.A. Berzofsky, J. Peisach, W.E. Blumberg, Sulfheme proteins. II. The reversible oxygenation of ferrous sulfmyoglobin, J. Biol. Chem. 246 (23) (1971) 7366–7372.
[13] J.A. Berzofsky, J. Peisach, J.O. Alben, Sulfheme proteins. 3. Carboxysulfmyoglobin: the relation between electron withdrawal from iron and ligand binding, J. Biol. Chem. 247 (12) (1972) 3774–3782.
[14] M. Brunori, D. Bourgeois, B. Vallone, The structural dynamics of myoglobin, J. Struct. Biol. 147 (3) (2004) 223–234.
[15] J.S. Olson, J. Soman, G.N. Phillips Jr, Ligand pathways in myoglobin: a review of Trp cavity mutations, IUBMB Life 59 (8–9) (2007) 552–562.
[16] A. Tomita, U. Kreutzer, S. Adachi, S.Y. Koshihara, T. Jue, 'It's hollow': the function of pores within myoglobin, J. Exp. Biol. 213 (Pt 16) (2010) 2748–2754.
[17] A. Tomita, T. Sato, K. Ichiyanagi, S. Nozawa, H. Ichikawa, M. Chollet, F. Kawai, S. Y. Park, T. Tsuduki, T. Yamato, et al., Visualizing breathing motion of internal cavities in concert with ligand migration in myoglobin, Proc. Natl. Acad. Sci. USA 106 (8) (2009) 2612–2616.
[18] R.F. Fischetti, D.J. Rodi, D.B. Gore, L. Makowski, Wide-angle X-ray solution scattering as a probe of ligand-induced conformational changes in proteins, Chem. Biol. 11 (10) (2004) 1431–1443.
[19] H.D. Mertens, D.I. Svergun, Structural characterization of proteins and complexes using small-angle X-ray solution scattering, J. Struct. Biol. 172 (1) (2010) 128–141.
[20] R.P. Rambo, J.A. Tainer, Characterizing flexible and intrinsically unstructured biological macromolecules by SAS using the Porod-Debye law, Biopolymers 95 (8) (2011) 559–571.
[21] H.L. Guedes, F.P. Silva Jr., C.C. Netto, C.M. de Salles, G. Alexandre, C.L. Oliveira,

I. Torriani, S.G. De Simone, Structural characterization and low-resolution model of BJ-48, a thrombin-like enzyme from *Bothrops jararacussu* venom, Biophys. Chem. 132 (2–3) (2008) 159–164.
[22] L. Makowski, J. Bardhan, D. Gore, J. Lal, S. Mandava, S. Park, D.J. Rodi, N.T. Ho, C. Ho, R.F. Fischetti, WAXS studies of the structural diversity of hemoglobin in solution, J. Mol. Biol. 408 (5) (2011) 909–921.
[23] R.G. Leon, H. Munier-Lehmann, O. Barzu, V. Baudin-Creuza, R. Pietri, J. Lopez-Garriga, C.L. Cadilla, High-level production of recombinant sulfide-reactive hemoglobin I from Lucina pectinata in Escherichia coli. High yields of fully functional holoprotein synthesis in the BLi5 *E. coli* strain, Protein Expr. Purif. 38 (2) (2004) 184–195.
[24] M. Allaire, L. Yang, Biomolecular solution x-ray scattering at the National Synchrotron Light Source, J. Synchrotron Radiat. 18 (2011) 41–44.
[25] M. Petoukhov, D. Franke, A. Shkumatov, G. Tria, A. Kikhney, M. Gajda, C. Gorba, H.D.T. Mertens, P.V. Konarev, D.I. Svergun, New developments in the ATSAS program package for small-angle scattering data analysis, J. Appl. Crystallogr. 45 (2012) 342–350.
[26] R. Pietri, S. Zerbs, D.M. Corgliano, M. Allaire, F.R. Collart, L.M. Miller, Biophysical and structural characterization of a sequence-diverse set of solute-binding proteins for aromatic compounds, J. Biol. Chem. 287 (28) (2012) 23748–23756.
[27] P.V. Konarev, V.V. Sokolova, M.H.J. Koch, D.I. Svergun, A. PRIMUS, Windows PC-based system for angle scattering drug analysis, J. Appl. Crystallogr. 36 (2003) 1277–1282.
[28] D.I. Svergun, Determination of the regularization parameter in indirect-transform methods using perceptual criteria, J. Appl. Crystallogr. 25 (1992) 495–503.
[29] D.I. Svergun, Restoring low resolution structure of biological macromolecules from solution scattering using simulated annealing, Biophys. J. 76 (1999) 2879–2886.
[30] V.V. Volkov, D.I. Svergun, Uniqueness of ab initio shape determination in small angle x-ray scattering, J. Appl. Crystallogr. 36 (2003) 860–864.
[31] M.B. Kozin, D.I. Svergun, Automated matching of high and low resolution structural models, J. Appl. Crystallogr. 34 (2001) 33–41.
[32] D.I. Svergun, C. Barberato, M.H.J. Koch, CRYSOL-A program to evaluate x-ray solution scattering of biological macromolecules from atomic coordinates, J. Appl. Crystallogr. 28 (1995) 768–773.
[33] L. Makowski, D. Gore, S. Mandava, D. Minh, S. Park, D.J. Rodi, R.F. Fischetti, X-ray solution scattering studies of the structural diversity intrinsic to protein ensembles, Biopolymers 95 (8) (2011) 531–542.
[34] L. Makowski, D.J. Rodi, S. Mandava, D.D. Minh, D.B. Gore, R.F. Fischetti, Molecular crowding inhibits intramolecular breathing motions in proteins, J. Mol. Biol. 375 (2) (2008) 529–546.
[35] D.W. Kraus, J.B. Wittenberg, Hemoglobins of the Lucina pectinata/bacteria symbiosis. I. Molecular properties, kinetics and equilibria of reactions with ligands, J. Biol. Chem. 265 (27) (1990) 16043–16053.
[36] H.S. Cho, N. Dashdorj, F. Schotte, T. Graber, R. Henning, P. Anfinrud, Protein structural dynamics in solution unveiled via 100-ps time-resolved x-ray scattering, Proc. Natl. Acad. Sci. USA 107 (16) (2010) 7281–7286.
[37] J.K. Krueger, G.A. Olah, S.E. Rokop, G. Zhi, J.T. Stull, J. Trewhella, Structures of calmodulin and a functional myosin light chain kinase in the activated complex: a neutron scattering study, Biochemistry 36 (20) (1997) 6017–6023.
[38] R. Kitahara, K. Hata, A. Maeno, K. Akasaka, M.S. Chimenti, E.B. Garcia-Moreno, M.A. Schroer, C. Jeworrek, M. Tolan, R. Winter, et al., Structural plasticity of staphylococcal nuclease probed by perturbation with pressure and pH, Proteins 79 (4) (2011) 1293–1305.
[39] D. Neves, L.F. Estrozi, V. Job, F. Gabel, G. Schoehn, A. Dessen, Conformational states of a bacterial alpha2-macroglobulin resemble those of human complement C3, PloS One 7 (4) (2012) e35384.
[40] M. Hammel, Validation of macromolecular flexibility in solution by small-angle X-ray scattering (SAXS), Eur. Biophys. J.: EBJ 41 (10) (2012) 789–799.
[41] F.A. Carvalho, J.W. Carvalho, P.S. Santiago, M. Tabak, Urea-induced unfolding of Glossoscolex paulistus hemoglobin, in oxy- and cyanomet-forms: a dissociation model, Int. J. Biol. Macromol. 52 (2013) 340–348.
[42] J.W. Carvalho, F.A. Carvalho, P.S. Santiago, M. Tabak, Thermal stability of extracellular hemoglobin of Rhinodrilus alatus (HbRa): DLS and SAXS studies, European Biophysics Journal, EBJ, 2016.
[43] M. Kozlowska, A. Tarczewska, M. Jakob, K. Szpotkowski, M. Wojtas, G. Rymarczyk, A. Ozyhar, Calponin-like Chd64 is partly disordered, PloS One 9 (5) (2014) e96809.
[44] T. Yokouchi, Y. Izumi, T. Matsufuji, Y. Jinbo, H. Yoshino, Unfolding intermediate of a multidomain protein, calmodulin, in urea as revealed by small-angle X-ray scattering, FEBS Lett. 551 (1–3) (2003) 119–122.
[45] T. Uzawa, S. Akiyama, T. Kimura, S. Takahashi, K. Ishimori, I. Morishima, T. Fujisawa, Collapse and search dynamics of apomyoglobin folding revealed by submillisecond observations of alpha-helical content and compactness, Proc. Natl. Acad. Sci. USA 101 (5) (2004) 1171–1176.
[46] M. Brunori, Myoglobin strikes back, Protien Sci. 19 (2) (2010) 195–201.
[47] R.J. Carrico, W.E. Blumberg, J. Peisach, The reversible binding of oxygen to sulfhemoglobin, J. Biol. Chem. 253 (20) (1978) 7212–7215.